Journal of Power Sources 218 (2012) 352–356

Contents lists available at SciVerse ScienceDirect

Journal of Power Sources

journal homepage: www.elsevier.com/locate/jpowsour

Short communication

Preparation of dual-pore anode supported Sc_2O_3-stabilized-ZrO_2 electrolyte planar solid oxide fuel cell by phase-inversion and dip-coating

Wang Sun [a], Naiqing Zhang [c,b], Yachun Mao [b,*], Kening Sun [b,c,*]

[a] Department of Chemistry, Harbin Institute of Technology, Harbin 150001, PR China
[b] Academy of Fundamental and Interdisciplinary Sciences, Harbin Institute of Technology, Harbin, 150001, PR China
[c] State Key Laboratory of Urban Water Resource and Environment, Harbin Institute of Technology, Harbin, 150090, PR China

HIGHLIGHTS

- Single cell presents a unique dual-pore anode structure.
- The dual-pore anode is fabricated by a facile and cost-effective phase-inversion technique in only one-step.
- The dual-pore anode reveals excellent rapid gas deliverability.
- Power output of 1.97 W cm^{-2} is obtained at 800 °C.

ARTICLE INFO

Article history:
Received 25 June 2012
Accepted 28 June 2012
Available online 14 July 2012

Keywords:
Solid oxide fuel cells
Anode-supported
Phase-inversion
Dip-coating
Scandia stabilized zirconia

ABSTRACT

In this paper, we report a dual-pore anode supported Sc_2O_3-stabilized-ZrO_2 (ScSZ) electrolyte planar SOFC with the cell configuration of Ni-YSZ|Ni-ScSZ|ScSZ|LSM-ScSZ|LSM prepared by a combination of phase-inversion and dip-coating. The Ni-YSZ anode substrate is fabricated by phase-inversion, exhibiting an asymmetric dual-pore structure. A Ni-ScSZ anode functional layer (AFL) is introduced between the ScSZ electrolyte and the Ni-YSZ anode substrate by dip-coating, a process aims at increasing the three-phase boundaries at the anode/electrolyte interface. A single cell with this unique anode structure is successfully fabricated, demonstrating maximum power densities of 0.76, 1.04, 1.32 and 1.97 W cm^{-2} at 650, 700, 750, and 800 °C, respectively, with humidified (3vol% H_2O) hydrogen as the fuel and oxygen as the oxidant. The microstructure morphologies of the SOFC are examined by SEM and comparisons of gas permeability for dual-pore and conventional anodes are also investigated.

1. Introduction

In order to alleviate global warming and environmental pollution, solid oxide fuel cells (SOFCs) have emerged as a novel clean energy production technique. Given the combined advantages of high conversion efficiency, flexible fuel requirement and low environmental impact they have been increasingly researched in recent years [1–3]. Tubular and planar configurations are two typical cell designs for SOFCs [4,5]. Compared with the tubular SOFC, the planar SOFC has several advantages such as shorter current paths, higher power density and reduced manufacturing cost [5–8].

In order to obtain a high power density at intermediate temperatures (≤1073 K), the anode-supported configuration is proposed because of the lower ohmic polarization from the thinner electrolyte [6–8]. The anode substrate is generally fabricated by ceramic manufacturing process such as tape-casting [9–11] or dry-pressing [12,13]. Anodes prepared by these two methods present a homogeneous structure. Alternatives such as graded anodes are fabricated by using different amounts of pore formers in each layer thus achieving a fine pore structure at the anode/electrolyte interface and more unhindered gas ch]annels in the anode substrate [14,15]. Such fabricating processes are complex and time-consuming.

Since the pioneering work by Loeb and Sourirajan [16], the phase-inversion technique has been widely used to fabricate gas separation membranes and hollow fibers [17–19]. In a typical phase inversion process, a solution consisting of polymer and solvent is immersed into a nonsolvent coagulation bath. Interchange of solvent and nonsolvent due to the diffusion causes the

* Corresponding authors. Academy of Fundamental and Interdisciplinary Sciences, Harbin Institute of Technology, Harbin, 150001, PR China. Tel./fax: +86 451 8641 2153.
E-mail addresses: ymao@hit.edu.cn (Y. Mao), keningsun@yahoo.com.cn (K. Sun).

0378-7753/$ – see front matter © 2012 Elsevier B.V. All rights reserved.
http://dx.doi.org/10.1016/j.jpowsour.2012.06.107

casting solution to go through a phase transition by which the membrane is formed [20]. Recently, micro-tubular SOFCs prepared by phase-inversion have been reported [21–24]. To date there has been little focus on planar SOFCs although. Jin et al. [25] fabricated an anode substrate for planar SOFC by phase-inversion. However, the maximum power density cell performance was only 0.38 W cm^{-2} at 800 °C.

In this paper, a Ni-YSZ anode substrate with a dual-pore structure has been prepared by phase-inversion in only one-step. Considering the higher ionic conductivity of Sc_2O_3 stabilized ZrO_2 (ScSZ) than that of Y_2O_3 stabilized ZrO_2 (YSZ) at intermediate-temperature [26], ScSZ was used as the electrolyte material. In an attempt to increase the three phase boundaries (TPBs) at electrolyte/anode interface the Ni-ScSZ anode functional layer (AFL) was introduced between the ScSZ electrolyte and the Ni-YSZ anode substrate by dip-coating. Finally, a single cell with a five-layer structure was successfully fabricated consisting of Ni-YSZ|Ni-ScSZ|ScSZ|LSM-ScSZ|LSM layers and exhibiting a unique anode structure and superior cell performance.

2. Experimental

The NiO-YSZ anode substrate with a dual-pore structure was prepared by phase-inversion. NiO (High Purity Chemicals, Japan) and 8YSZ (TZ-8Y, Tosoh Co., Japan) powders (NiO:YSZ = 60:40 by weight) were used as the anode materials. Corn starch was used as the pore former. Polyethersulfone (PESf, E2010, BASF, Germany) was used as the binder. *N*-methyl-2-pyrrolidone (NMP) and polyvinylpyrrolidone (PVP) were employed as the solvent and dispersant, respectively. NiO, YSZ and corn starch were added into the polymer solution prepared by dissolving PESf and PVP into NMP. The mixtures were ball-milled for 48 h to obtain the well-dispersed slurry. The slurry was degassed for 20min, after which it was poured into a round mold (diameter of 20 mm). The mold was immersed into deionized water for 24 h. The as-prepared membrane was then dried overnight. Finally, the sample was pre-calcined at 1100 °C for 2 h.

NiO and 10 mol%Sc_2O_3–ZrO_2 (ScSZ, Tero Chemical Co., China) were the materials used for the anode functional layer (AFL). The NiO-ScSZ AFL and thin ScSZ electrolyte film were prepared by dip-coating, as described elsewhere [27]. After the ScSZ dip-coating process, the anode and ScSZ film were co-sintered at 1,400 °C for 6 h. $La_{0.8}Sr_{0.2}MnO_3$ (LSM, Nextech, USA) and ScSZ powders were used as the cathode materials. The LSM-ScSZ cathode functional layer (LSM:ScSZ = 60:40 by weight) and the LSM current collecting layer were fabricated by the screen-printing method, and then sintered at 1200 °C for 2 h. Finally, a single cell with the aforementioned five-layer structure of Ni-YSZ|Ni-ScSZ|ScSZ|LSM-ScSZ|LSM was obtained.

The microstructures of the cell were characterized by scanning electron microscopy (SEM, FEI Quanta 200F, Netherlands). Gas permeation tests were performed using nitrogen gas (99.99% pure N_2) at gauge pressures of between 0.5×10^5 Pa and 2.5×10^5 Pa at room temperature. The nitrogen flow rate was measured by a thermal mass flowmeter (5886, NICETY, China). Before the gas permeation test, the anodes were reduced at 800 °C. The electrochemical performance of the cells was measured by Arbin Equipment (USA) with 50 sccm of humidified (3vol% H_2O) hydrogen as the fuel and 100 sccm oxygen as the oxidant. An electrochemical system (PARSTAT 2273) was employed for EIS measurement. The impedance frequency range was from 10 mHz to 1 MHz with a signal amplitude of 10 mV.

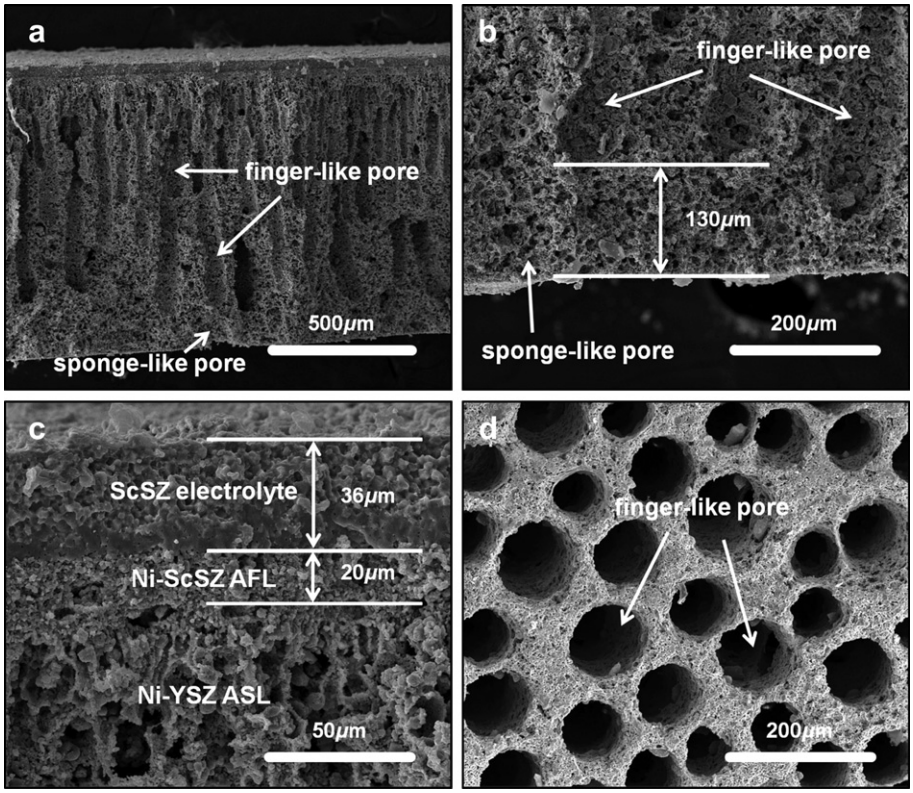

Fig. 1. Cross-sectional SEM images of the electrolyte/anode half cell after testing: (a) overall view; (b) interface of sponge-like pores and finger-like pores, (c) electrolyte/anode interface, and (d) surface of finger-like pores.

3. Results and discussion

Fig. 1a) presents the cross sectional morphology of the electrolyte/anode half cell after testing. It can be seen that Ni-YSZ anode substrate exhibits an asymmetric dual-pore structure. The finger-like pores provide convenient channels for fuel gas diffusion. The formation mechanism of the finger-like pores can be explained by the viscous fingering phenomenon [28,29]. Under the finger-like porous layer, there is a sponge-like porous layer. As shown in Fig. 1b), the finger-like pores are orthogonal to the sponge-like porous layer, and these layers are coherent. The thickness of the sponge-like porous layer is about 130 μm Fig. 1c) shows the interfacial microstructure of the electrolyte and the anode. A 36-μm-thick ScSZ electrolyte film was successfully fabricated on the anode. The ScSZ electrolyte is dense without any cracks, and adheres well to the Ni-ScSZ AFL. The thickness of the Ni-ScSZ AFL is about 20 μm. Again the Ni-ScSZ AFL and the finger-like porous layer of the Ni-YSZ anode substrate are coherent. It also can be observed that the finger-like pores are also orthogonal to the Ni-ScSZ AFL. Such a structure could facilitate the fuel gas distribution throughout the TPBs in the Ni-ScSZ AFL. In addition, the microstructure of Ni-ScSZ AFL is much finer than that of the finger-like porous layer, and the decreased pore sizes will be beneficial for expanding TPBs at the anode/electrolyte interface. The surface morphology of the finger-like pores (prepared by removing the sponge-like porous layer) presents a honeycomb skeleton structure, and one finger-like pore is round and interconnected, as shown in Fig. 1d).

The pore structure of the porous media influences the gas permeability. The anode substrate as the thickest component of the anode-supported SOFC should have sufficient unhindered pores for the fuel gas diffusion. Fig. 2 shows the comparison of the gas permeabilities of the dual-pore anode with pore former (marked as DPA-A), the dual-pore anode without pore former (marked as DPA-B), the finger-like porous layer (prepared by removing the sponge-like porous layer) and the conventional anode prepared by tape-casting (marked as TPA) [11]. The finger-like porous layer presents the highest gas permeability, indicating that the finger-like pores are good channels for fuel gas diffusion, as shown in Fig. 2. The gas permeabilities of DPA-B are higher than that of TPA and much lower than that of the finger-like porous layer at different pressures. The sponge-like pores with lower porosity confine the fuel transport, resulting in the lower gas permeability of DPA-B. In order to increase the porosity of the sponge-like pores, corn starch was added as pore former. It can be seen that the gas permeabilities of DPA-A are much higher than that of DPA-B at all pressure ranges. For example, the value of the gas permeability of DPA-A is about one third of that of finger-like porous layer and 23 times of that of TPA at 1.0 bar, respectively.

Fig. 3 shows the discharge curves of the cell measured at 650–800 °C, the maximum power densities reach 0.76, 1.04, 1.32 and 1.97 W cm^{-2} at 650, 700, 750, and 800 °C, respectively. The performance is much higher than that observed in previous study of planar cell prepared by phase inversion (0.383 W cm^{-2}) at 800 °C [25]. The maximum power density is also higher than that of the cell prepared by tape-casting (1.41 W cm^{-2} [30]) at 800 °C. The dual-pore anode delivered excellent fast gas deliverability property, as previously mentioned. Therefore there is sufficient fuel gas entering the anode active region through the anode substrate, which is involved in the electrochemical reaction at the anode/electrolyte interface.

In order to further evaluate the performance of the cell, the electrochemical impedance spectra (*EIS*) were investigated under OCV conditions, as shown in Fig. 4. The intercepts of the impedance arcs on the real axis at high frequencies correspond to the ohmic resistance (R_Ω), and the intercepts with the real axis in the low-frequency region represent the total resistance (R_T). The overall size of the impedance loop is attributed to the interface resistance (R_P), including activation polarization and concentration polarization. As shown in Fig. 4, the total and ohmic resistances decrease with increasing operating temperatures. Each curve consists of a small higher-frequency arc and a large lower-frequency arc at different operating temperatures. And these arcs decrease in size with increasing temperature. In previous studies, the low-frequency arc was attributed to cathode polarization and the anode reaction resistance determined the high-frequency arc [31,32]. Therefore, we believe that the cathode dominates the low-frequency cell polarization resistance.

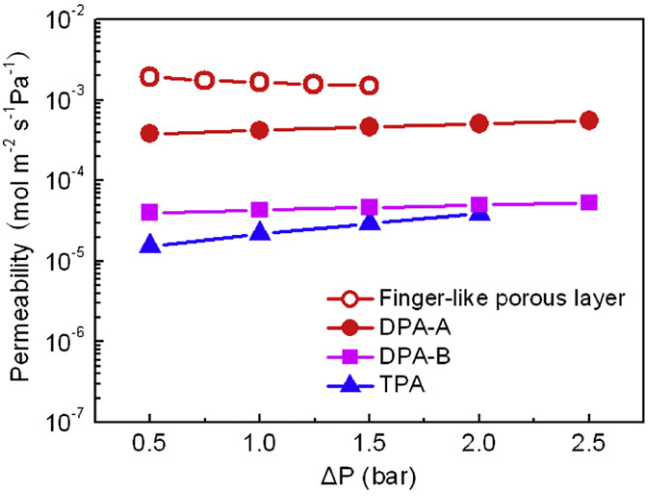

Fig. 2. Gas permeation data of dual-pore anodes, finger-like porous layer and tape-casting anode.

Fig. 5a) shows the interface resistances (R_P) and ohmic resistances (R_Ω) of the dual-pore anode supported cell. As the operating temperatures increase from 650 to 800 °C, the total resistances decrease from 0.486 to 0.156 Ω cm^2 while the ohmic resistances decrease from 0.093 to 0.058 Ω cm^2. This can be explained by the increased ionic conductivity of the electrolyte and faster electrode kinetics. The resistances are much lower than that observed in previous studies (R_T is ~0.92 Ω cm^2 with R_Ω of ~0.15 Ω cm^2 [25] and R_T is 0.47 Ω cm^2 with R_Ω of 0.11 Ω cm^2 [30]). The temperature dependences of the interface resistances and ohmic resistances are

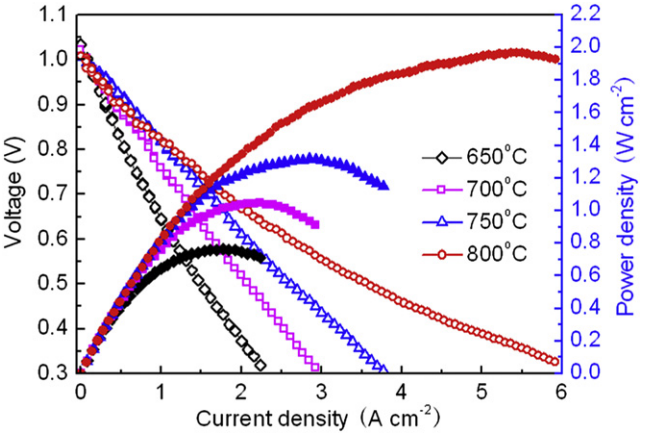

Fig. 3. Current–voltage characteristics and the corresponding power densities as a function of current densities for dual-pore anode supported SOFC.

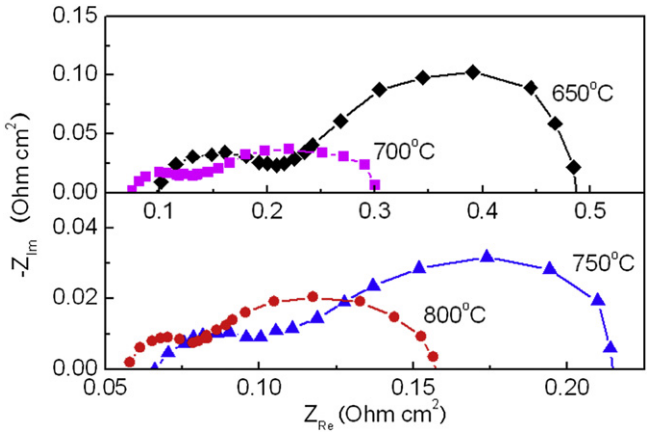

Fig. 4. Impedance spectra for the cell measured under the OCV conditions.

plotted in Fig. 5b). The data could be well formulated by using Arrhenius equation [33]. The activation energies belong to the interface resistance and ohmic resistance can be obtained base on the slopes of two fitting lines in Fig. 5b). The activation energy of the interface resistance is 75.8 kJ mol^{-1} and the activation energy for the ohmic resistance is 25.1 kJ mol^{-1}. High performances and reduced resistances in this work are mainly attributed to the unique anode structure and enhanced ion transport across the electrolyte as well as optimized electrode/electrolyte interface.

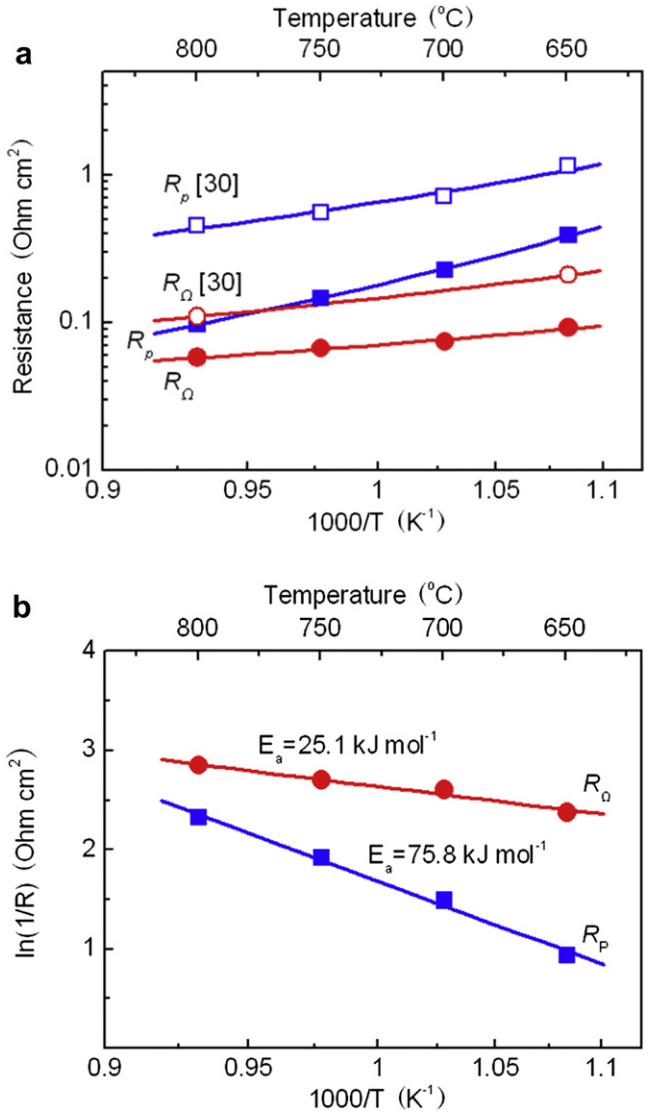

Fig. 5. (a) Interface resistances (R_p) and ohmic resistances (R_Ω) of the dual-pore anode and conventional anode; (b) temperature dependence of R_p and R_Ω.

4. Conclusions

A dual-pore anode supported ScSZ-electrolyte SOFC was successfully fabricated by a combination of phase-inversion and dip-coating. The Ni-YSZ anode substrate was prepared by a facile phase-inversion technique, presenting a dual-pore structure which contained a finger-like porous layer and a sponge-like porous layer. Compared with the conventional anode prepared by tape-casting, the dual-pore anode showed good fast gas deliverability property. The Ni-ScSZ AFL was dip-coated on the finger-like porous layer, expanding the TPBs at the electrolyte/anode interface. The finger-like pores are orthogonal to the Ni-ScSZ AFL. Such a structure facilitates the fuel gas distribution throughout the TPBs in the AFL. A single cell was successfully fabricated, demonstrating the maximum power densities of 0.76, 1.04, 1.32 and 1.97 W cm^{-2} at 650, 700, 750, and 800 °C, respectively. The combination of phase-inversion and dip-coating offers a novel approach to prepare planar SOFC with unique anode structure and superior cell performance.

Acknowledgment

This work was financially supported by State Key Laboratory of Urban Water Resource and Environment, Harbin Institute of Technology (No. 2008TS04).

References

[1] B.C.H. Steele, A. Heinzel, Nature 414 (2001) 345.
[2] T. Suzuki, Z. Hasan, Y. Funahashi, T. Yamaguchi, Y. Fujishiro, M. Awano, Science 325 (2009) 852.
[3] L. Yang, C.D. Zuo, S.Z. Wang, K. Blinn, M.F. Liu, Z. Liu, Z. Cheng, M.L. Liu, Science 326 (2009) 126.
[4] N.M. Sammes, Y. Du, R. Bove, Journal of Power Sources 145 (2005) 428.
[5] T.L. Wen, D. Wang, H.Y. Tu, M. Chen, Z. Lu, Z. Zhang, H. Nie, W. Huang, Solid State Ionics 152-153 (2002) 399.
[6] S.D. Kim, S.H. Hyun, J. Moon, J.H. Kim, R.H. Song, Journal of Power Sources 139 (2005) 67.
[7] F. Zhao, A.V. Virkar, Journal of Power Sources 141 (2005) 79.
[8] A.V. Virkar, J. Chen, C.W. Tanner, J.W. Kim, Solid State Ionics 131 (2000) 189.
[9] X.F. Ye, S.R. Wang, Q. Hu, Z.R. Wang, T.L. Wen, Z.Y. Wen, Electrochemistry Communications 11 (2009) 823.
[10] M. Mukhopadhyay, J. Mukhopadhyay, A.D. Sharma, R.N. Basu, International Journal of Hydrogen Energy 37 (2012) 2524.
[11] H. Moon, S.D. Kim, S.H. Hyun, H.S. Kim, International Journal of Hydrogen Energy 33 (2008) 1758.
[12] N. Ai, Z. Lü, K.F. Chen, X.Q. Huang, X.B. Du, W.H. Su, Journal of Power Sources 171 (2007) 489–494.
[13] K.F. Chen, X.J. Chen, Z. Lü, N. Ai, X.Q. Huang, W.H. Su, Electrochimica Acta 53 (2008) 7825.
[14] P. Holtappels, C. Sorof, M.C. Verbraeken, S. Rambert, U. Vogt, Fuel Cells 06 (2006) 113.
[15] A.C. Müller, D. Herbstritt, E. Ivers-Tiffée, Solid State Ionics 152-153 (2002) 537.
[16] S. Loeb, S. Sourirajan, Advances in Chemistry Series 38 (1962) 117.
[17] J.C. Jansen, M.G. Buonomenna, A. Figoli, E. Drioli, Desalination 193 (2006) 58.
[18] D.T. Clausi, W.J. Koros, Journal of Membrane Science 167 (2000) 79.
[19] J.C. Jansen, M. Macchione, E. Drioli, Journal of Membrane Science 255 (2005) 167.
[20] T.H. Young, L.W. Chen, Desalination 103 (1995) 233.
[21] N.T. Yang, X.Y. Tan, Z.F. Ma, Journal of Power Sources 183 (2008) 14.
[22] C.H. Yang, C. Jin, F.L. Chen, Electrochemistry Communications 12 (2010) 657.
[23] C.L. Yang, W. Li, S.Q. Zhang, L. Bi, R.R. Peng, C.S. Chen, W. Liu, Journal of Power Sources 187 (2009) 90.
[24] X.Z. Zhang, B. Lin, Y.H. Ling, Y.C. Dong, G.Y. Meng, X.Q. Liu, International Journal of Hydrogen Energy 35 (2010) 8654.
[25] C. Jin, C.H. Yang, F.L. Chen, Journal of Membrane Science 363 (2010) 250.

[26] T.H. Etsel, S.N. Flengas, Chemical Reviews 70 (1970) 339.
[27] Z.H. Wang, K.N. Sun, S.Y. Shen, N.Q. Zhang, J.S. Qiao, P. Xu, Journal of Membrane Science 320 (2008) 500.
[28] W. Sun, N.Q. Zhang, Y.C. Mao, K.N. Sun, Electrochemistry Communications 20 (2012) 117.
[29] B.F.K. Kingsbury, K. Li, Journal of Membrane Science 328 (2009) 134.
[30] Z.W. Wang, M.J. Cheng, Y.L. Dong, M. Zhang, H.M. Zhang, Journal of Power Sources 156 (2006) 306.
[31] J.H. Koh, Y.S. Yoo, J.W. Park, H.C. Lim, Solid State Ionics 149 (2002) 157.
[32] Y.B. Lin, Z.L. Zhan, J.L. Liu, S.A. Barnett, Solid State Ionics 176 (2005) 1827.
[33] S. Kim, Y.L. Yang, R. Christoffersen, A.J. Jacobson, Solid State Ionics 104 (1997) 57.